The Astronomical Journal, 127:3399–3410, 2004 June

THE VARIABILITY OF SAGITTARIUS A* AT CENTIMETER WAVELENGTHS

Robeson M. Herrnstein,[1] Jun-Hui Zhao,[2] Geoffrey C. Bower,[3] and W. M. Goss[4]
Received 2003 December 8; accepted 2004 February 23

ABSTRACT

We present the results of a 3.3 yr project to monitor the flux density of Sagittarius A* at 2.0, 1.3, and 0.7 cm with the Very Large Array. Between 2000.5 and 2003.0, 119 epochs of data were taken with a mean separation between epochs of 8 days. After 2003.0, observations were made roughly once per month for a total of nine additional epochs. Details of the data calibration process are discussed, including corrections for opacity and elevation effects, as well as changes in the flux density scales between epochs. The fully calibrated light curves for Sgr A* at all three wavelengths are presented. Typical errors in the flux density are 6.1%, 6.2%, and 9.2% at 2.0, 1.3, and 0.7 cm, respectively. There is preliminary evidence for a bimodal distribution of flux densities, which may indicate the existence of two distinct states of accretion onto the supermassive black hole. At 1.3 and 0.7 cm, there is a tail in the distribution toward high flux densities. Significant variability is detected at all three wavelengths, with the largest amplitude variations occurring at 0.7 cm. The rms deviation of the flux density of Sgr A* is 0.13, 0.16, and 0.21 Jy at 2.0, 1.3, and 0.7 cm, respectively. During much of this monitoring campaign, Sgr A* appeared to be relatively quiescent compared with results from previous campaigns. At no point during the monitoring campaign did the flux density of Sgr A* more than double its mean value. The mean spectral index of Sgr A* is $\alpha = 0.20 \pm 0.01$ (where $S_\nu \propto \nu^\alpha$), with a standard deviation of 0.14. The spectral index appears to depend linearly on the observed flux density at 0.7 cm with a steeper index observed during outbursts. This correlation is consistent with the expectation for outbursts that are self-absorbed at wavelengths of 0.7 cm or longer and inconsistent with the effects of simple models for interstellar scintillation. Much of the variability of Sgr A*, including possible time lags between flux density changes at the different wavelengths, appears to occur on timescales less than the time resolution of our observations (8 days). Future observations should focus on the evolution of the flux density on these time-scales.

Key words: accretion, accretion disks — black hole physics — Galaxy: center — radio continuum: galaxies

1. INTRODUCTION

Observations of stellar proper motions in the central $1''$ (0.04 pc) of the Milky Way suggest that a $4 \times 10^6\ M_\odot$ black hole is located at the dynamical center of the Galaxy (Schödel et al. 2002; Ghez et al. 2003b). In the radio, the bright ($\sim$1 Jy), compact source called Sagittarius A* (Sgr A*) appears to be closely associated with the supermassive black hole (Menten et al. 1997). For over two decades, the radio flux density of Sgr A* has been known to vary (Brown & Lo 1982), but the cause of this variability remains unclear. The radio variability tends to increase toward shorter wavelengths, and significant fluctuations on roughly weekly timescales are observed at wavelengths of 2 cm and shorter (Zhao, Bower, & Goss 2001). Based on this observed increase in fractional variability toward shorter wavelengths, the variability of Sgr A* at centimeter wavelengths has been suggested to be intrinsic to the source (Zhao et al. 1992). At millimeter and submillimeter wavelengths, the flux density of Sgr A* is even more variable (Wright & Backer 1993; Tsuboi, Miyazaki, & Tsutsumi 1999; Zhao et al. 2003). Changes of up to a factor of 4 in the flux density have been observed at 1.3 mm using the Sub-Millimeter Array (SMA) (Zhao et al. 2003).

Short-term variability of Sgr A* has been detected in X-rays. In 2002, a multiwavelength campaign was undertaken to simultaneously monitor Sgr A* at centimeter, millimeter, infrared, and X-ray wavelengths. Based on 500 ks of *Chandra* observations, Baganoff (2003) finds that flares of a factor of $\sim$10 occur roughly once per day. (In this paper, we call events on hour-to-day timescales "flares," while events on time-scales of weeks are referred to as "outbursts.") The strongest X-ray flare during this observation occurred on 2002 May 29 and showed a factor of 20 increase in the flux of Sgr A*. To date, three additional large X-ray flares have been observed between 2000 June and 2003 October. On 2000 October 27, the flux of Sgr A* detected by *Chandra* increased by a factor of 45 during a 10 ks flare (Baganoff et al. 2001). A factor of 20 increase in the flux of Sgr A* at 2–10 keV was detected by *XMM-Newton* during the beginning of a flare on 2001 September 4, but the observations unfortunately did not include the entire event (Goldwurm et al. 2003). More recently, a factor of 160 flare lasting 2.7 ks was detected with *XMM-Newton* on 2002 October 3 (Porquet et al. 2003).

Recently, Sgr A* has been detected for the first time at infrared wavelengths. In the infrared, Sgr A* appears to show both long-term and short-term variability. The short-term variability occurs on timescales of $\sim$1 hr, similar to the timescale of X-ray events (Genzel et al. 2003). The day to week timescale of the long-term infrared variability is more similar to the timescale of radio outbursts (Ghez et al. 2003b).

[1] Department of Astronomy, Mail Code 5246, Columbia University, 550 West 120th Street, New York, NY 10027; herrnstein@astro.columbia.edu.
[2] Harvard-Smithsonian Center for Astrophysics, 60 Garden Street, Cambridge, MA 02138; jzhao@cfa.harvard.edu.
[3] Radio Astronomy Lab, 601 Campbell Hall, University of California, Berkeley, CA 94720; gbower@astron.berkeley.edu.
[4] National Radio Astronomy Observatory, P.O. Box 0, Socorro, NM 87801; mgoss@aoc.nrao.edu.

In order to understand the detailed nature of the variability of Sgr A* in the radio, Zhao et al. (2001, hereafter ZBG01) combined Very Large Array[5] (VLA) data from frequent monitoring of Sgr A* between 1990.1 and 1993.5 (Zhao et al. 1992) with 20 yr of additional archival data from 1977 to 1999. At 1.3 cm, the flux density of Sgr A* typically varied by 30%, and occasional outbursts of 100% were observed. A comparison of the light curves at 20, 6.0, 3.6, 2.0, and 1.3 cm showed that the largest amplitude variations in flux density occurred at the shortest wavelengths (ZBG01).

Using a maximum entropy method (Press et al. 1989), as well as a classic periodogram augmented with CLEAN to search for periodicities, ZBG01 found a periodicity of 106 ± 10 days [$1.1(\pm 0.1) \times 10^{-7}$ Hz] at 3.6, 2.0, and 1.3 cm. The light curves were consistent with no phase offset between the three wavelengths. The mean profile of the 106 day cycle at 1.3 cm had a broad peak, roughly 25 ± 5 days wide at full width at half-maximum (FWHM), indicating that the variability of Sgr A* is most likely quasi-periodic in nature. Analysis of data presented in ZBG01 was hindered, however, by highly irregular sampling intervals. Observations were only made on a regular basis (with sampling intervals from 1 to 28 days) between 1990.1 and 1991.5, a small fraction of the entire study. Between 1991.5 and 1993.5, the sampling was less frequent with a maximum sampling interval of 120 days. Gaps in the archival data were as large as 1200 days.

Additional evidence for periodic variability on the order of 100 days has been detected at 2 and 3 mm using 46 epochs of data taken between 1996 and 2000 with the Nobeyama Millimeter Array (Tsutsumi, Miyazaki, & Tsuboi 2002). When the data are folded with a period of 106 days, the resulting cycle divides roughly equally into a ''high'' and ''low'' activity state. During the high activity state, the flux density of Sgr A* can vary by as much as a factor of 3, while Sgr A* is relatively quiescent in the low activity state.

Evidence for a period of 57 days was suggested by Falcke (1999) based on 11 cm data from the Green Bank Interferometer. This result suggested that the 106 day periodicity could be a harmonic of a higher frequency periodicity. Due to sparse sampling over much of the 20 yr baseline, the data presented by ZBG01 were not sensitive to periods shorter than $\sim$50 days. A new monitoring campaign in which the flux density of Sgr A* was regularly monitored on weekly timescales was necessary to search for these short periodicities and detect the shape of outbursts and phase offsets between the different wavelengths.

From 2000 June to 2003 October, over 170 hours of VLA observing time were used to monitor the flux density of Sgr A* at 2.0, 1.3, and 0.7 cm. The results of this 3.3 yr project are presented in this paper. Section 3 explains in detail the data calibration, including corrections for opacity effects and errors in absolute flux calibration. The fully calibrated flux densities for Sgr A* at 2.0, 1.3, and 0.7 cm are presented in § 4 and are also listed in their entirety in Table 2. The characteristics of the light curve, including the spectral index and time delay between wavelengths, are also discussed.

This paper deals primarily with data calibration and the general characteristics of the light curve and spectrum. Results from the analysis of these data for periodic or quasi-periodic signals will be presented in subsequent papers. Although § 4 briefly compares our light curves with those from monitoring campaigns at other wavelengths, detailed comparisons are presented elsewhere. Zhao et al. (2003) compares the radio light curve with preliminary data from the Sub-Millimeter Array. A separate paper also discusses evidence for correlated events in the radio and X-ray and possible implications for accretion models for Sgr A* (Zhao et al. 2004). Finally, six Very Long Baseline Array observations were made as part of this monitoring campaign. The results from these observations are presented in Bower et al. (2004).

2. OBSERVATIONS

Data were collected in the A, B, C, D, and hybrid configurations of the VLA through projects AZ 128 (2000 June 21–September 26), AZ 129 (2000 October 5–2001 September 27), AZ 136 (2001 October 2–2003 January 4), and AZ 143 (2003 January 13–2003 October 14). From 2000.5 to 2003.0, the flux density of Sgr A* at 2.0, 1.3, and 0.7 cm was measured roughly once per week (for a total of 119 epochs). Between 2003.0 and 2003.8, nine additional observations were made once per month in order to increase our sensitivity to long-term periodicities. Although a total of 128 observations were made, problems with weather or instrumentation resulted in the occasional loss of data at one or more wavelengths. Successful flux densities were measured for a total of 115 epochs at 2.0 cm, 124 epochs at 1.3 cm, and 121 epochs at 0.7 cm. Sampling intervals in the finely sampled data range from 1 to 26 days with a mean separation of 8 days (and a median separation of 7 days). Observations after 2003.0 have a mean and median separation of 30 days. The resulting data are sensitive to periods between roughly 15 and 2000 days.

A typical observation lasted a total of 1–2 hr. Either 3C 286 or 3C 48 served as the primary flux calibrator, and 1741−312 (J1744−312) and 1817−254 (J1820−254) were used to track the phase during the observations. (B1950.0 name conventions are used throughout this paper.) Following an observation of the flux calibrator at 3.6 cm to calibrate offsets in the pointing solutions, four minute integrations were made at 2.0, 1.3, and 0.7 cm. The pointing offsets were then recalculated for 1741−312. Because of the close proximity of the sources, these solutions were also applied to Sgr A* and 1817−254. Observations of Sgr A* at all three wavelengths were interleaved between observations of a phase calibrator at roughly 15 minute intervals. A total of 5–15 minutes of integration time on Sgr A* were obtained at each wavelength for each observation.

3. DATA REDUCTION

Initial calibration of the data was performed using the Astronomical Image Processing System (AIPS). Data from antennas and baselines with large rms noise were flagged. At all three wavelengths, the data were corrected for changes in efficiency as a function of elevation using the most recent gain curves for each antenna. Prior to 2001 July 25, the gain curves at 2.0 and 1.3 cm were applied using the NRAO supplied tasks, FIXUGAIN and FIXKGAIN. At 0.7 cm, gain corrections were applied using an algorithm we developed specifically for this project. The task also allowed us to correct the 0.7 cm data for losses due to high opacity at low elevation. Because opacity effects should be negligible at

[5] The National Radio Astronomy Observatory is a facility of the National Science Foundation operated under cooperative agreement by Associated Universities, Inc.

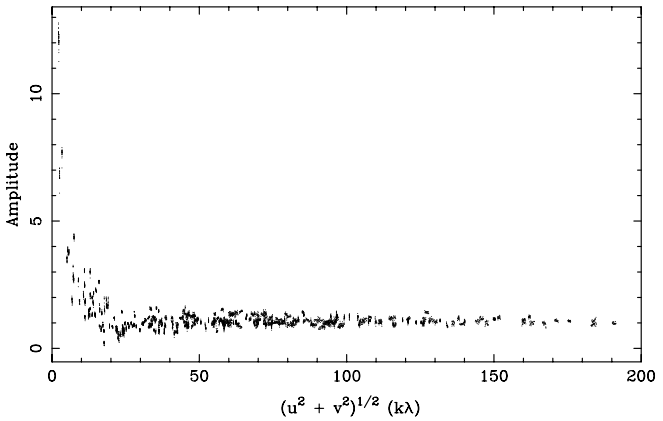

FIG. 1.—Plot of amplitude (in janskys) vs. (u, v)-distance for Sgr A*. This data was taken at a wavelength of 1.3 cm on 2002 December 19 in the C Array of the VLA. Contributions from Sgr A West are negligible on baselines longer than $\sim$40 kλ.

longer wavelengths, this correction was not applied to the 2.0 and 1.3 cm data. Beginning 2001 July 25, both the opacity and gain corrections were incorporated directly into the AIPS task FILLM. These corrections are equivalent to our previous method, and we subsequently used FILLM to apply opacity and gain corrections to all of our data.

Primary flux density calibration was performed using 3C 286 (1328+307), except for 11 epochs where observations later than 20:00 local sidereal time (LST) forced us to use 3C 48 (0134+329). When 3C 48 was observed, baselines from 0 to 40 kλ were used in the flux density calibration for all three wavelengths. For all other epochs, the flux density calibration was performed using 3C 286 and included all baselines longer than 150 kλ at 2.0 cm or 185 kλ at 1.3 cm. At both wavelengths, solutions were calculated using 30 s integration times. At 0.7 cm, a model image of 3C 286 obtained from C. Chandler of NRAO was used in the flux density calibration, thus allowing the inclusion of all baselines. First, a phase-only flux density calibration was performed using a solution interval equal to the integration time (10 s). The final calibration included both amplitude and phase with a 30 s solution interval. The flux density scale calculated from 3C 286 or 3C 48 was applied to 1741$-$312 and 1817$-$254. Phase calibrator flux densities and associated errors for the phase calibrators were measured using the AIPS task GETJY.

The flux density of Sgr A* was measured in the (u, v)-domain. In determining the flux density of Sgr A*, it is important to avoid contributions from the extended source, Sgr A West, that surrounds the supermassive black hole. In Figure 1, a plot of amplitude versus (u, v)-distance for Sgr A* shows the contribution from Sgr A West on baselines $\lesssim$40 kλ at 1.3 cm (angular scales $\gtrsim 5''$). For observations made in the largest configurations of the VLA, only baselines longer than 100 kλ (corresponding to a $2''$ resolution) were used in the flux density calculation. For more compact arrays, it was necessary to decrease the minimum allowed (u, v)-distance for the longer wavelength data. At 2.0 cm in C Array and 1.3 cm in D Array, the minimum (u, v)-distance was 60 kλ. In D Array, baselines longer than 40 kλ were used for 2.0 cm data. Finally, an initial estimate of the uncertainty in the flux density of Sgr A* was calculated assuming that Sgr A* has the same fractional error in flux density ($\Delta S/S$) as the phase calibrators.

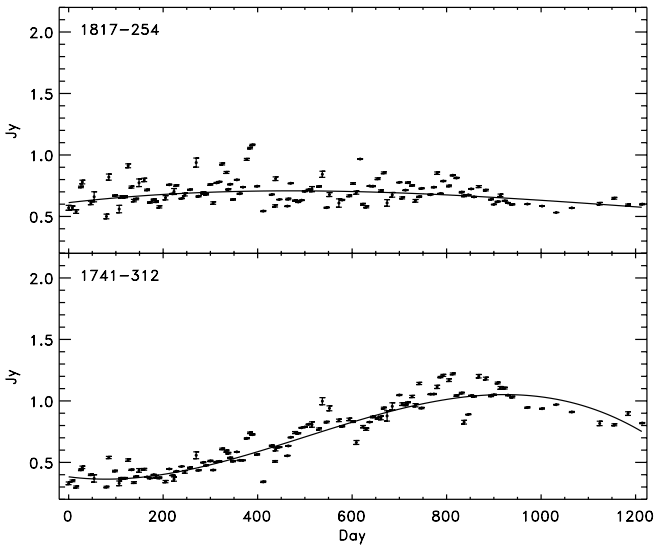

FIG. 2.—Flux density of 1817$-$254 *(top)* and 1741$-$312 *(bottom)* at 1.3 cm after calibration in AIPS. The best cubic fit to the data is overlaid. The vertical axis is chosen to match Fig. 5.

3.1. *Correcting for Systematic Scaling Errors in the Flux Density Calibration*

We present 1.3 cm flux densities for 1817$-$254 and 1741$-$312 after initial calibration in AIPS in Figure 2. Variability in flux density of the two calibrators is due to a long-term drift in flux density, short-term variability intrinsic to the source, and slight differences in the absolute flux density scale between epochs. In the following paragraphs, we present the method used to calculate and correct for systematic changes in the flux density scale between epochs. Because the intrinsic short-term variability of the calibrators is not known, we assume that calibrators have only long-term drifts in flux density. Short-term variability, which is highly correlated between the two calibrators, is assumed to result from changes in the flux density scale between epochs. These scale factors are quantified and removed from the data. If any intrinsic, short-term variability of the calibrators exists, it is accounted for in the calculation of the final uncertainties in these scale factors presented at the end of this section.

3.1.1. *Calculation of Gain Adjustment Factors*

To estimate the long-term drift in flux density, a cubic fit has been made to the light curve of each calibrator (see Fig. 2). The parameters of the best-fit model for 1817$-$254 and 1741$-$312 at each wavelength are given in Table 1. At all three wavelengths, 1741$-$312 is consistent with a cubic profile. Calibrator 1817$-$254, however, shows little long-term change in flux over our entire monitoring campaign. This is reflected by the relatively small values of the linear, quadratic, and cubic terms for this calibrator (see Table 1).

Both phase calibrators show additional short-term variability that is not accounted for by the cubic model. For each epoch, the ratio of the model flux density to the observed flux density is calculated for each calibrator. If we define calibrator 1 as 1817$-$254 and calibrator 2 as 1741$-$312, then these ratios are given by

$$g_1 = S_1/S_1', \qquad g_2 = S_2/S_2', \tag{1}$$

TABLE 1
CUBIC FIT PARAMETERS OF PHASE CALIBRATOR

Phase Calibrator	Observing Band (cm)	a_0 (mJy)	a_1 (mJy yr^{-1})	a_2 (mJy yr^{-2})	a_3 (mJy yr^{-3})
1817−254	2.0	794 ± 6	47 ± 10	-80 ± 10	17 ± 8
	1.3	612 ± 5	162 ± 8	-78 ± 6	8 ± 5
	0.7	388 ± 5	5 ± 8	-82 ± 6	-26 ± 5
1741−312	2.0	540 ± 5	-444 ± 10	542 ± 7	-117 ± 7
	1.3	383 ± 5	-182 ± 9	459 ± 5	-112 ± 5
	0.7	287 ± 6	-163 ± 10	419 ± 5	-105 ± 5

NOTE.—The cubic fit is of the form $S_\nu = a_0 + a_1 x + a_2 x^2 + a_3 x^3$, where x is measured in years and $x = 0$ corresponds to day 0 in Table 2.

where S_i is the model flux density from the cubic fit, and S_i' is the observed flux density. The uncertainty in g_i is calculated as the quadrature sum of the uncertainty in the observed flux density and the uncertainty in the model flux density from the cubic fit. Figure 3 shows a plot of g_1 and g_2 for every epoch during the monitoring campaign. Intrinsic short-term variability of the two calibrators should result in uncorrelated values of g_1 and g_2. Systematic errors in the absolute flux density scale, however, will appear as a correlation between the two ratios in Figure 3. The values of g_1 and g_2 are well-correlated, indicating that systematic errors in the absolute flux density calibration are a significant component of the calibrator variability.

We calculate a gain adjustment factor (GAF) as the weighted average of g_1 and g_2:

$$g = \frac{g_1/\sigma_{g_1}^2 + g_2/\sigma_{g_2}^2}{1/\sigma_{g_1}^2 + 1/\sigma_{g_2}^2}. \quad (2)$$

The gain adjustment factors track the systematic change in the flux density scale with time. The GAF "light curve" at 1.3 cm is shown as the solid line in Figure 3. At all three wavelengths, the average value of the GAF is close to 1, indicating that there is no systematic underestimate or overestimate of the flux densities. However, the typical size of the fractional correction increases toward shorter wavelengths. The standard deviation of g is 0.07, 0.11, and 0.17 at 2.0, 1.3, and 0.7 cm, respectively.

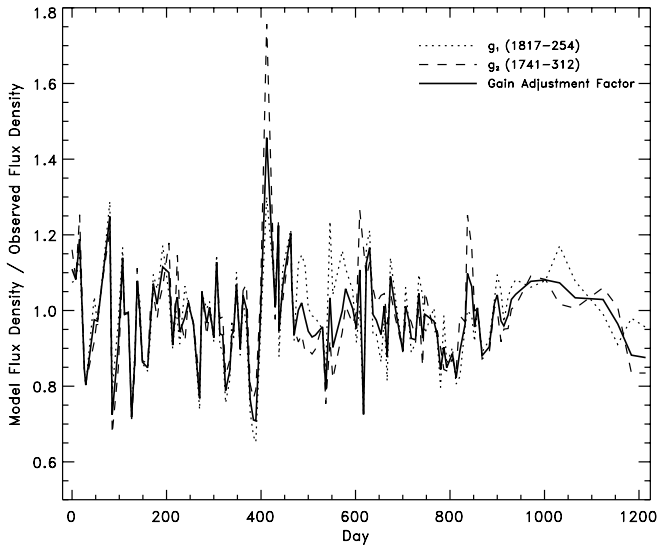

FIG. 3.—Ratio of model flux density derived from the cubic fit to the observed flux density at 1.3 cm for 1817−254 (g_1) and 1741−312 (g_2). The GAF, calculated as the weighted mean of g_1 and g_2 at each epoch, is overlaid as a solid line (see § 3.1.1).

3.1.2. *Estimation of Uncertainties*

Typical errors in flux density reported by AIPS range from 1% to 3%. The fact that the values of g_1 and g_2 are not identical to within these errors (see, e.g., day 486–515 in Fig. 3) indicates that AIPS has underestimated the true uncertainties in the flux density measurements and/or there is significant intrinsic variability of one or both of the phase calibrators. The errors reported by AIPS are statistical and do not include contributions from systematic errors. Due to these systematic errors (e.g., pointing errors), the flux density calibration at any given epoch is expected to be accurate to only 5%–10%. The intrinsic variability of the two phase calibrators is not known. Therefore, while both an underestimation of the errors by AIPS and intrinsic source variability probably contribute to the difference between g_1 and g_2, we take the conservative approach and assume that all of the residual variability observed is due to systematic errors in the calibration.

Assuming that the phase calibrators have only slow drifts in flux density and no short-term variability to within the noise, the difference between g_1 and g_2 in Figure 3 can be used to estimate the true rms noise, σ', in the flux density measurements. This assumption is reasonable for both of our calibrators (see Fig. 4). An additional error, calculated as some fraction, f, of the source flux density, is added in quadrature to the initial error reported by AIPS. For epoch i,

$$\sigma'(i) = \sqrt{[f S_\nu(i)]^2 + \sigma_{\rm AIPS}(i)^2}. \quad (3)$$

The value of f is chosen such that the fit of the GAFs to the residual variability of the two calibrators has a reduced χ^2 of one. The values of f for our data are 0.059, 0.057, and 0.078 for 2.0, 1.3, and 0.7 cm, respectively. Final errors in the flux density measurements for Sgr A* are typically 6.1%, 6.2%, and 9.2% for 2.0, 1.3, and 0.7 cm, respectively.

A gain adjustment factor could not be determined for the observation on 2003 June 16. In this case, we calculate the uncertainty in the flux density measurement as the quadrature sum of the mean uncertainty in the fully calibrated flux densities of Sgr A* and the mean size of the gain adjustment factors.

3.1.3. *Final Light Curves*

Fully calibrated flux densities for 1817−254 and 1741−312 are calculated by multiplying the observed flux density by the

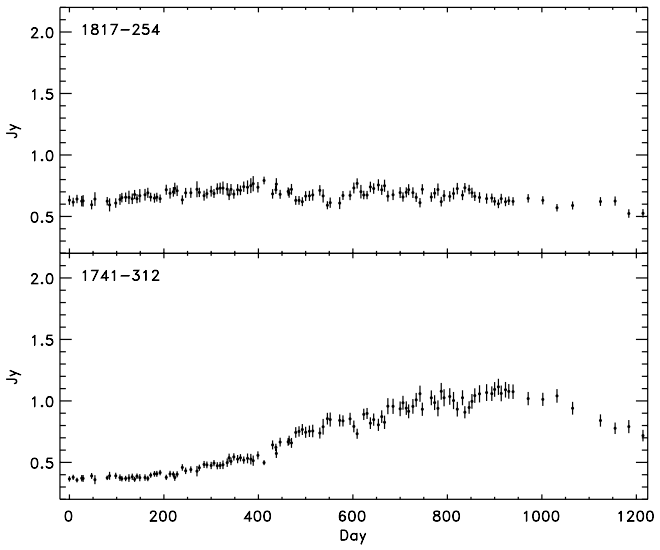

FIG. 4.—Flux density of 1817−254 *(top)* and 1741−312 *(bottom)* at 1.3 cm after application of the gain adjustment factors. Error bars include the original error and the additional fractional error discussed in § 3.1.2. The vertical axis is chosen to match Fig. 5.

gain adjustment factor. The resulting light curves at 1.3 cm are shown in Figure 4. After application of the GAF, the flux densities of both phase calibrators show only long-term drifts to within the uncertainties. For each epoch, the final flux density and associated uncertainty for Sgr A* is calculated in the same way as for the phase calibrators and is equal to gS'_*.

4. RESULTS

Figure 5 shows the radio light curves of Sgr A* at 2.0, 1.3, and 0.7 cm. The fully calibrated flux densities and associated errors are listed in Table 2. A machine readable version of Table 2 is available through the on-line version of this article. Table 3 summarizes the characteristics of the variability of Sgr A* at each wavelength.

Table 4 shows the mean and standard deviation of the flux density of Sgr A* as a function of the VLA array in which the observations were made. VLA configurations are changed roughly every 4 months, with slight variations due to subscription and scheduling. The 16 month cycle begins in the largest configuration (A) and moves to progressively smaller configurations, ending in the D configuration. As the antennas are moved to a new configuration, roughly 3 weeks are spent in a hybrid array, during which the northern arm of the array remains in the previous (more extended) configuration and the eastern and western arms are in the new (more compact) configuration. These hybrid arrays are used primarily for sources at low declinations. At the end of the cycle, roughly 3 weeks are spent moving the antennas from the D configuration back to the A configuration. Because the scheduling of configuration changes and the time spent in each configuration can vary by as much as 2–3 weeks, we do not expect the changes in configuration to produce periodic signatures in our data. This point will be discussed in more detail when the

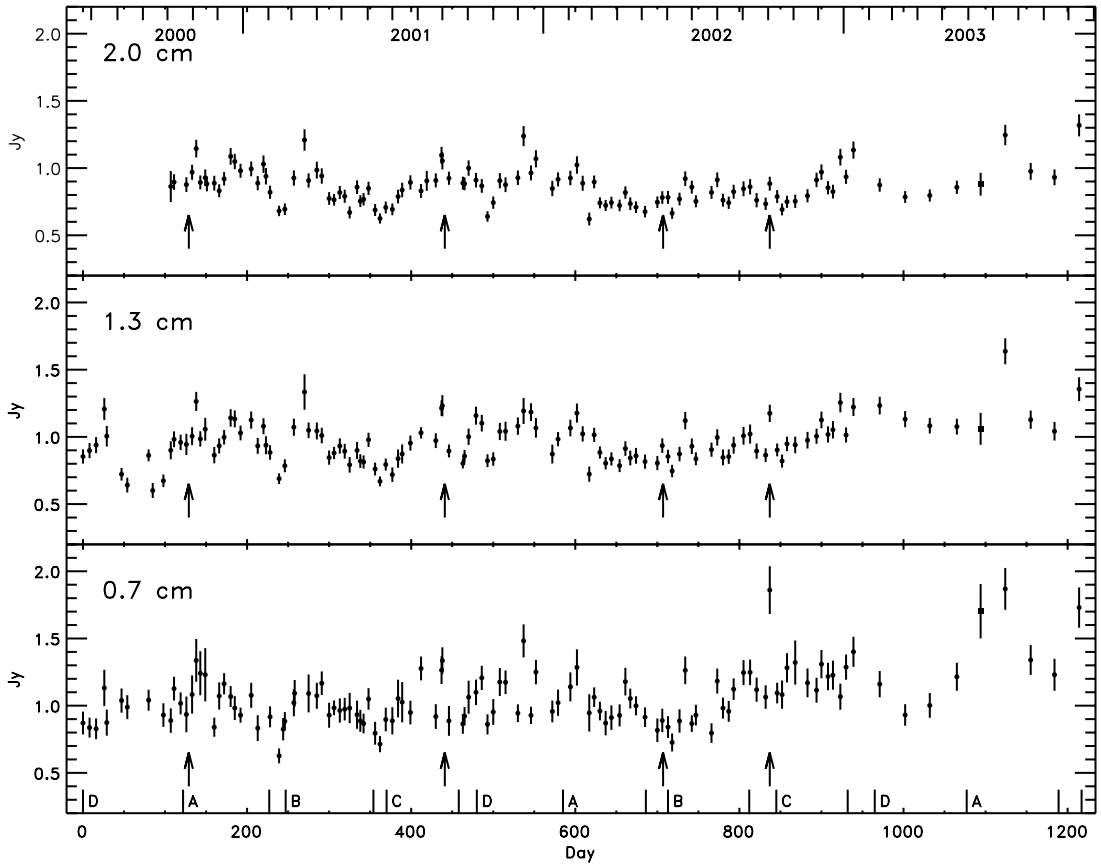

FIG. 5.—Intrinsic variability of Sgr A* at 2.0, 1.3, and 0.7 cm. The corresponding date is labeled in the top panel, and the VLA configuration is labeled in the bottom panel. Hybrid configurations are not labeled. Arrows mark four large X-ray flares (see § 1).

TABLE 2

CALIBRATED FLUX DENSITY OF Sgr A*

Date	Project Day[a]	2.0 cm (Jy)	1.3 cm (Jy)	0.7 cm (Jy)	Spectral Index
2000 Jun 21	0	...	0.85 ± 0.05	0.87 ± 0.09	...
2000 Jun 29	8	...	0.90 ± 0.06	0.84 ± 0.07	...
2000 Jul 7	16	...	0.94 ± 0.06	0.83 ± 0.08	...
2000 Jul 17	26	...	1.21 ± 0.08	0.13 ± 0.14	...
2000 Jul 20	29	...	1.00 ± 0.08	0.87 ± 0.10	...
2000 Aug 6	47	...	0.72 ± 0.05	0.04 ± 0.09	...
2000 Aug 14	54	...	0.64 ± 0.06	0.99 ± 0.09	...
2000 Sep 8	80	...	0.86 ± 0.04	0.04 ± 0.08	...
2000 Sep 13	85	...	0.60 ± 0.06	...	...
2000 Sep 26	98	...	0.67 ± 0.05	0.93 ± 0.09	...
2000 Oct 5	107	0.86 ± 0.12	0.90 ± 0.07	0.89 ± 0.09	0.01 ± 0.15
2000 Oct 9	111	0.90 ± 0.06	0.98 ± 0.06	1.13 ± 0.09	0.22 ± 0.10
2000 Oct 17	119	...	0.96 ± 0.06	1.02 ± 0.08	...
2000 Oct 24	126	0.88 ± 0.06	0.94 ± 0.08	0.94 ± 0.13	0.08 ± 0.14
2000 Oct 31	133	0.97 ± 0.06	1.00 ± 0.07	1.08 ± 0.14	0.10 ± 0.13
2000 Nov 5	138	1.15 ± 0.07	1.26 ± 0.07	1.34 ± 0.16	0.17 ± 0.12
2000 Nov 10	143	0.89 ± 0.05	0.99 ± 0.06	1.24 ± 0.16	0.29 ± 0.13
2000 Nov 16	149	0.93 ± 0.06	1.06 ± 0.09	1.23 ± 0.20	0.28 ± 0.15
2000 Nov 18	151	0.88 ± 0.06	...	...	...
2000 Nov 27	160	0.89 ± 0.06	0.86 ± 0.06	0.84 ± 0.07	-0.05 ± 0.10
2000 Dec 3	166	0.83 ± 0.05	0.93 ± 0.06	1.07 ± 0.10	0.24 ± 0.10
2000 Dec 9	172	0.92 ± 0.05	1.00 ± 0.05	1.16 ± 0.08	0.22 ± 0.08
2000 Dec 17	180	1.09 ± 0.06	1.14 ± 0.07	1.07 ± 0.08	-0.02 ± 0.09
2000 Dec 22	185	1.05 ± 0.06	1.13 ± 0.06	0.98 ± 0.09	-0.04 ± 0.10
2000 Dec 29	192	0.98 ± 0.05	1.03 ± 0.06	0.93 ± 0.06	-0.06 ± 0.08
2001 Jan 11	205	0.99 ± 0.06	1.13 ± 0.06	1.08 ± 0.09	0.09 ± 0.10
2001 Jan 19	213	0.89 ± 0.05	0.93 ± 0.06	0.83 ± 0.10	-0.03 ± 0.12
2001 Jan 26	220	1.03 ± 0.07	1.08 ± 0.06	...	...
2001 Jan 29	223	0.94 ± 0.06	0.94 ± 0.07	...	...
2001 Feb 3	228	0.82 ± 0.05	0.88 ± 0.05	0.92 ± 0.08	0.11 ± 0.10
2001 Feb 14	239	0.68 ± 0.04	0.69 ± 0.04	0.63 ± 0.06	-0.07 ± 0.10
2001 Feb 19	244	...	...	0.83 ± 0.08	...
2001 Feb 21	246	0.69 ± 0.04	0.79 ± 0.05	0.88 ± 0.07	0.23 ± 0.09
2001 Mar 4	257	0.93 ± 0.06	1.07 ± 0.06	1.02 ± 0.10	0.12 ± 0.11
2001 Mar 5	258	...	...	1.09 ± 0.10	...
2001 Mar 17	270	1.21 ± 0.08	1.33 ± 0.13	...	...
2001 Mar 22	275	0.91 ± 0.05	1.05 ± 0.06	1.09 ± 0.14	0.22 ± 0.12
2001 Apr 1	285	0.99 ± 0.06	1.04 ± 0.06	1.07 ± 0.10	0.08 ± 0.10
2001 Apr 7	291	0.94 ± 0.06	1.01 ± 0.06	1.17 ± 0.09	0.20 ± 0.09
2001 Apr 16	300	0.77 ± 0.05	0.85 ± 0.05	0.93 ± 0.09	0.18 ± 0.11
2001 Apr 22	306	0.76 ± 0.04	0.88 ± 0.05	0.98 ± 0.06	0.23 ± 0.07
2001 Apr 29	313	0.82 ± 0.05	0.93 ± 0.06	0.96 ± 0.09	0.17 ± 0.10
2001 May 5	319	0.79 ± 0.05	0.89 ± 0.06	0.97 ± 0.08	0.20 ± 0.10
2001 May 11	325	0.67 ± 0.05	0.79 ± 0.06	0.98 ± 0.11	0.36 ± 0.12
2001 May 20	334	0.86 ± 0.05	0.90 ± 0.06	0.93 ± 0.11	0.08 ± 0.12
2001 May 24	338	0.75 ± 0.04	0.82 ± 0.05	0.89 ± 0.08	0.16 ± 0.10
2001 May 28	342	0.77 ± 0.05	0.81 ± 0.05	0.87 ± 0.07	0.11 ± 0.10
2001 Jun 3	348	0.85 ± 0.05	0.98 ± 0.05	1.05 ± 0.08	0.20 ± 0.09
2001 Jun 11	356	0.69 ± 0.04	0.76 ± 0.05	0.80 ± 0.09	0.15 ± 0.12
2001 Jun 17	362	0.63 ± 0.04	0.67 ± 0.04	0.71 ± 0.06	0.13 ± 0.10
2001 Jun 24	369	0.71 ± 0.04	0.79 ± 0.05	0.90 ± 0.09	0.23 ± 0.11
2001 Jul 2	377	0.69 ± 0.04	0.72 ± 0.05	0.89 ± 0.10	0.22 ± 0.12
2001 Jul 9	384	0.79 ± 0.05	0.84 ± 0.07	1.05 ± 0.14	0.25 ± 0.13
2001 Jul 14	389	0.84 ± 0.05	0.87 ± 0.07	1.03 ± 0.15	0.17 ± 0.14
2001 Jul 24	399	0.89 ± 0.05	0.95 ± 0.06	0.95 ± 0.09	0.06 ± 0.10
2001 Aug 5	412	0.83 ± 0.05	1.03 ± 0.04	1.28 ± 0.09	0.40 ± 0.09
2001 Aug 13	419	0.91 ± 0.07	...	...	...
2001 Aug 24	430	0.91 ± 0.05	0.97 ± 0.06	0.92 ± 0.09	0.03 ± 0.11
2001 Aug 31	437	1.10 ± 0.06	1.21 ± 0.06	1.26 ± 0.10	0.14 ± 0.09
2001 Sep 1	438	1.05 ± 0.06	1.23 ± 0.08	1.34 ± 0.10	0.22 ± 0.09
2001 Sep 9	446	0.92 ± 0.05	0.90 ± 0.05	0.89 ± 0.11	-0.05 ± 0.12
2001 Sep 26	463	0.89 ± 0.05	0.80 ± 0.04	0.87 ± 0.07	-0.04 ± 0.09
2001 Sep 28	465	0.88 ± 0.05	0.86 ± 0.05	0.92 ± 0.07	0.04 ± 0.09
2001 Oct 3	470	1.00 ± 0.06	1.00 ± 0.06	1.06 ± 0.12	0.05 ± 0.12
2001 Oct 11	479	0.91 ± 0.05	1.16 ± 0.07	1.10 ± 0.10	0.20 ± 0.10

TABLE 2—*Continued*

Date	Project Day[a]	2.0 cm (Jy)	1.3 cm (Jy)	0.7 cm (Jy)	Spectral Index
2001 Oct 18	486	0.87 ± 0.05	1.10 ± 0.06	1.21 ± 0.09	0.31 ± 0.09
2001 Oct 25	493	0.64 ± 0.04	0.82 ± 0.05	0.86 ± 0.08	0.29 ± 0.10
2001 Nov 1	500	0.74 ± 0.05	0.84 ± 0.05	0.95 ± 0.10	0.24 ± 0.11
2001 Nov 9	508	0.91 ± 0.06	1.04 ± 0.06	1.18 ± 0.10	0.25 ± 0.10
2001 Nov 18	515	0.88 ± 0.06	1.04 ± 0.07	1.17 ± 0.09	0.27 ± 0.09
2001 Dec 1	530	0.93 ± 0.05	1.08 ± 0.07	0.94 ± 0.07	0.01 ± 0.09
2001 Dec 8	537	1.24 ± 0.08	1.19 ± 0.10	1.48 ± 0.12	0.17 ± 0.10
2001 Dec 17	546	0.96 ± 0.06	1.18 ± 0.07	0.93 ± 0.06	-0.05 ± 0.08
2001 Dec 23	552	1.07 ± 0.06	1.07 ± 0.07	1.25 ± 0.09	0.15 ± 0.09
2002 Jan 12	572	0.85 ± 0.06	0.87 ± 0.07	0.96 ± 0.08	0.11 ± 0.10
2002 Jan 19	579	0.92 ± 0.05	0.98 ± 0.05	1.02 ± 0.10	0.11 ± 0.10
2002 Feb 3	594	0.93 ± 0.05	1.07 ± 0.06	1.14 ± 0.11	0.21 ± 0.10
2002 Feb 11	602	1.02 ± 0.07	1.18 ± 0.07	1.29 ± 0.14	0.23 ± 0.11
2002 Feb 18	609	0.89 ± 0.06	1.02 ± 0.06	...	...
2002 Feb 26	617	0.62 ± 0.05	0.72 ± 0.06	0.95 ± 0.14	0.39 ± 0.15
2002 Mar 4	623	0.90 ± 0.05	1.01 ± 0.05	1.06 ± 0.07	0.16 ± 0.08
2002 Mar 11	630	0.74 ± 0.04	0.88 ± 0.05	0.96 ± 0.07	0.25 ± 0.09
2002 Mar 18	637	0.72 ± 0.04	0.80 ± 0.05	0.87 ± 0.09	0.19 ± 0.11
2002 Mar 25	644	0.74 ± 0.04	0.84 ± 0.05	0.91 ± 0.09	0.20 ± 0.11
2002 Apr 4	654	0.72 ± 0.04	0.79 ± 0.05	0.93 ± 0.08	0.23 ± 0.10
2002 Apr 11	661	0.82 ± 0.05	0.91 ± 0.05	1.18 ± 0.10	0.34 ± 0.10
2002 Apr 17	667	0.74 ± 0.05	0.84 ± 0.06	1.05 ± 0.07	0.34 ± 0.09
2002 Apr 24	674	0.71 ± 0.04	0.86 ± 0.06	1.00 ± 0.07	0.32 ± 0.09
2002 May 5	685	0.68 ± 0.04	0.82 ± 0.05	0.91 ± 0.07	0.28 ± 0.10
2002 May 20	700	0.75 ± 0.04	0.81 ± 0.05	0.82 ± 0.09	0.10 ± 0.11
2002 May 26	706	0.78 ± 0.05	0.94 ± 0.05	0.89 ± 0.09	0.15 ± 0.11
2002 Jun 2	713	0.78 ± 0.05	0.85 ± 0.05	0.84 ± 0.08	0.08 ± 0.11
2002 Jun 7	718	0.66 ± 0.04	0.75 ± 0.05	0.73 ± 0.07	0.09 ± 0.11
2002 Jun 16	727	0.77 ± 0.05	0.87 ± 0.05	0.89 ± 0.09	0.15 ± 0.11
2002 Jun 23	734	0.92 ± 0.05	1.12 ± 0.06	1.26 ± 0.10	0.30 ± 0.09
2002 Jul 1	742	0.86 ± 0.05	0.93 ± 0.06	0.87 ± 0.06	0.01 ± 0.09
2002 Jul 6	747	0.75 ± 0.05	0.84 ± 0.05	0.93 ± 0.08	0.20 ± 0.10
2002 Jul 25	766	0.82 ± 0.05	0.91 ± 0.05	0.80 ± 0.07	-0.01 ± 0.10
2002 Aug 1	773	0.91 ± 0.06	1.00 ± 0.06	1.18 ± 0.09	0.24 ± 0.09
2002 Aug 8	780	0.76 ± 0.05	0.85 ± 0.06	0.98 ± 0.08	0.24 ± 0.10
2002 Aug 15	787	0.74 ± 0.05	0.85 ± 0.05	0.96 ± 0.08	0.24 ± 0.10
2002 Aug 20	793	0.82 ± 0.05	0.94 ± 0.06	1.12 ± 0.08	0.29 ± 0.09
2002 Sep 1	805	0.85 ± 0.06	1.01 ± 0.07	1.25 ± 0.09	0.36 ± 0.09
2002 Sep 10	813	0.86 ± 0.06	1.02 ± 0.07	1.25 ± 0.10	0.35 ± 0.09
2002 Sep 18	821	0.76 ± 0.05	0.89 ± 0.06	1.12 ± 0.09	0.36 ± 0.10
2002 Sep 28	832	0.73 ± 0.05	0.86 ± 0.05	1.06 ± 0.09	0.35 ± 0.10
2002 Oct 3	837	0.88 ± 0.05	1.18 ± 0.06	1.86 ± 0.18	0.70 ± 0.10
2002 Oct 12	846	0.79 ± 0.05	0.90 ± 0.05	1.09 ± 0.08	0.31 ± 0.09
2002 Oct 18	852	0.69 ± 0.04	0.82 ± 0.05	1.08 ± 0.11	0.42 ± 0.11
2002 Oct 24	858	0.75 ± 0.05	0.95 ± 0.05	1.28 ± 0.11	0.51 ± 0.10
2002 Nov 3	868	0.75 ± 0.05	0.94 ± 0.06	1.32 ± 0.16	0.53 ± 0.13
2002 Nov 18	883	0.79 ± 0.05	0.98 ± 0.06	1.17 ± 0.11	0.37 ± 0.10
2002 Nov 29	894	0.91 ± 0.05	1.00 ± 0.06	1.12 ± 0.09	0.19 ± 0.10
2002 Dec 5	900	0.97 ± 0.06	1.13 ± 0.06	1.31 ± 0.11	0.28 ± 0.09
2002 Dec 13	908	0.85 ± 0.05	1.02 ± 0.06	1.22 ± 0.10	0.34 ± 0.10
2002 Dec 19	914	0.83 ± 0.05	1.05 ± 0.07	1.23 ± 0.11	0.38 ± 0.10
2002 Dec 28	923	1.08 ± 0.06	1.25 ± 0.07	1.07 ± 0.10	0.02 ± 0.10
2003 Jan 4	930	0.94 ± 0.05	1.01 ± 0.06	1.29 ± 0.09	0.30 ± 0.09
2003 Jan 13	939	1.13 ± 0.06	1.22 ± 0.07	1.40 ± 0.11	0.20 ± 0.09
2003 Feb 14	971	0.87 ± 0.05	1.23 ± 0.07	1.16 ± 0.10	0.30 ± 0.10
2003 Mar 17	1002	0.79 ± 0.04	1.13 ± 0.06	0.93 ± 0.08	0.21 ± 0.10
2003 Apr 16	1032	0.80 ± 0.05	1.08 ± 0.06	1.00 ± 0.09	0.27 ± 0.10
2003 May 19	1065	0.86 ± 0.05	1.08 ± 0.06	1.22 ± 0.10	0.34 ± 0.10
2003 Jun 16	1094	0.88 ± 0.09	1.06 ± 0.12	1.70 ± 0.20	0.62 ± 0.14
2003 Jul 16	1124	1.25 ± 0.08	1.64 ± 0.10	1.87 ± 0.16	0.39 ± 0.10
2003 Aug 16	1155	0.98 ± 0.06	1.13 ± 0.07	1.34 ± 0.11	0.30 ± 0.10
2003 Sep 14	1184	0.93 ± 0.06	1.04 ± 0.07	1.23 ± 0.12	0.26 ± 0.11
2003 Oct 14	1214	1.32 ± 0.08	1.36 ± 0.09	1.73 ± 0.15	0.25 ± 0.10

[a] Project day 0 is 2000 June 21. Days refer to LST days such that observations occurred at roughly the same time each day.

TABLE 3
PARAMETERS FOR THE FLUX DENSITY VARIABILITY OF Sgr A*

Wavelength (cm)	Number of Epochs	$\langle S_\nu \rangle$ (Jy)	$S_{\rm min}$ (Jy)	$S_{\rm max}$ (Jy)	σ (Jy)	χ_r^2 of Fit to Constant S_ν
2.0.....	115	0.834 ± 0.005	0.62 ± 0.05	1.32 ± 0.08	0.13	5.7
1.3.....	124	0.926 ± 0.005	0.60 ± 0.06	1.64 ± 0.10	0.16	6.7
0.7.....	121	1.001 ± 0.008	0.63 ± 0.06	1.87 ± 0.16	0.21	3.9

NOTES.—The error in the mean flux density is calculated as the weighted error from all measurements. The standard deviation of the measured flux densities at each wavelength is given as σ.

data are analyzed for periodicities, but we can conclude from Table 4 that no trends in flux density or variability as a function of observing array are apparent.

Figure 6 plots a histogram of the flux densities at each wavelength using a bin size of 0.05 Jy. This bin size is roughly equal to the mean uncertainty in the flux density of Sgr A* at 2.0 and 1.3 cm. Uncertainties in the distribution are calculated as the square root of the number of points in each bin. At all three wavelengths, there appears to be a tendency toward a bimodal distribution of flux densities. If the bimodal distribution is real, it may reflect two different states of accretion onto the supermassive black hole.

Significant variability in the flux density is observed at all three wavelengths (see Fig. 5). The reduced χ^2 of a fit of a constant flux density to the observed light curve was calculated at each wavelength. The reduced χ^2 is equal to 5.7 at 2.0 cm, 6.7 at 1.3 cm, and 3.9 at 0.7 cm. The similar shape of the three light curves indicates that the flux densities at centimeter wavelengths are also highly correlated. Figure 6 shows high flux density tails in the distributions at 1.3 and 0.7 cm. These tails reflect the increased variability toward shorter wavelengths, consistent with the results of Zhao et al. (1992). The largest variability in flux densities was observed at 0.7 cm, where the flux density of Sgr A* varied from a minimum value of 0.63 ± 0.06 Jy to a maximum value of 1.86 ± 0.16 Jy. The flux density of Sgr A* has a standard deviation during our monitoring campaign of 0.13, 0.16, and 0.21 Jy at 2.0, 1.3, and 0.7 cm, respectively.

A comparison of our light curves to the regularly sampled data from ZBG01 indicates that Sgr A* may have been in a relatively quiescent state from 2000.5 to 2003.8. Between 1990.1 and 1991.5, ZBG01 monitored the flux density of Sgr A* with sampling intervals ranging from 1 to 28 days. These finely sampled data form a small subset of the entire 20 yr ZBG01 data set. During the 1.4 yr of regular observations, two outbursts in which the 1.3 cm flux density of Sgr A* exceeded twice the mean value were observed. At least three additional outbursts of smaller amplitude were also observed.

Strong outbursts appear to be less frequent in the recent monitoring data. We observed no outbursts in which the flux density of Sgr A* doubled. Only one outburst at 2.0 cm had an amplitude greater than 50% higher than the mean flux density (0.834 ± 0.005 Jy). This outburst occurred on 2003 October 14 and had a flux density of 1.32 ± 0.08 Jy. At 1.3 cm, the largest outburst was a 4.5 σ event on 2003 July 16 (day 1124). On this date, the flux density of Sgr A* was 1.64 ± 0.10 Jy, 77% higher than the mean value during our monitoring campaign (0.926 ± 0.005 Jy). At 0.7 cm, we detected two 4.1 σ outbursts in which the flux density of Sgr A* was $\sim$86% higher than the mean value (1.001 ± 0.008 Jy). An outburst with a flux density of 1.86 ± 0.18 Jy occurred on 2002 October 3 (day 837), followed by a second outburst on 2003 July 16 (day 1124) with a flux density of 1.87 ± 0.16 Jy. Although there are relatively few strong outbursts overall, many of the largest outbursts at all three wavelengths occurred within the past year. This result suggests that Sgr A* may have become more active beginning in mid 2003.

Initial comparison of the radio light curves with X-ray observations of Sgr A* indicates that there may be a correlation between strong X-ray flares and increases in the flux density at centimeter wavelengths. The dates of the four strong X-ray flares discussed in § 1 are marked by arrows in Figure 5. In particular, VLA observations made on 2002 October 3, just 13.5 hr after the onset of the factor of 160 flare, show highly elevated flux densities at all three wavelengths. The 0.7 cm flux density for this date (1.86 ± 0.18 Jy) was one of the two largest flux densities measured during our entire campaign. This date also marked the steepest measured spectral index

TABLE 4
FLUX DENSITY AS A FUNCTION OF ARRAY

	2.0 cm			1.3 cm			0.7 cm		
CONFIGURATION	Number of Epochs	$\langle S_\nu \rangle$ (Jy)	σ (Jy)	Number of Epochs	$\langle S_\nu \rangle$ (Jy)	σ (Jy)	Number of Epochs	$\langle S_\nu \rangle$ (Jy)	σ (Jy)
A.....	33	0.86	0.14	32	0.96	0.17	29	1.03	0.24
BnA.....	6	0.77	0.24	6	0.83	0.23	7	0.83	0.35
B.....	26	0.81	0.11	26	0.91	0.12	26	0.97	0.13
CnB.....	7	0.73	0.09	7	0.83	0.17	7	0.95	0.38
C.....	21	0.85	0.12	20	0.97	0.14	20	1.13	0.15
DnC.....	5	0.94	0.11	5	0.94	0.18	5	1.01	0.21
D.....	17	0.85	0.13	28	0.93	0.17	27	1.00	0.16

NOTES.—The standard deviation is calculated from the spread of measured flux densities for that array. BnA refers to the hybrid array of the VLA with the northern arm in the A configuration (see § 4).

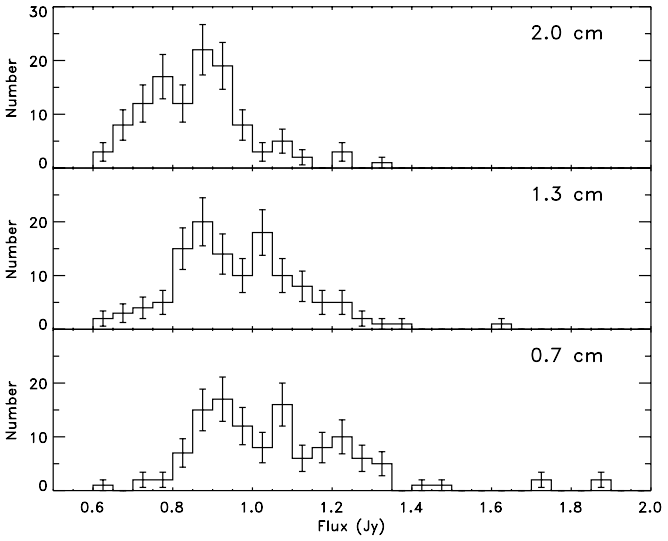

FIG. 6.—Histogram of flux densities at each wavelength. The bin size is 50 mJy. At all three wavelengths, the distribution of flux densities shows evidence for two distinct peaks. A high flux density tail is apparent at 1.3 and 0.7 cm, reflecting the increased variability toward shorter wavelengths.

(0.70 ± 0.10, see § 4.1). Correlated X-ray and radio variability may provide clues to the underlying physical processes near the supermassive black hole. Comparison of the radio and X-ray light curves, including a discussion of the relationship between the radio and X-ray events on 2002 October 3, is presented in detail in Zhao et al. (2004).

Recent observations of Sgr A* with the SMA indicate that submillimeter and centimeter flux densities are also correlated. The SMA (operated jointly by the Smithsonian Astrophysical Observatory and the Academica Sinica Institute for Astronomy and Astrophysics) is the first interferometric array to work full-time at wavelengths $\lesssim$1 mm. The high resolution of this interferometer will allow Sgr A* to be separated from the surrounding thermal dust emission from Sgr A West. Although still under construction at the time, monitoring of the flux density of Sgr A* at 1.3 mm began in 2001 (Zhao et al. 2003). Between 2001 March and 2002 July, the flux density of Sgr A* was measured at 24 epochs with a resolution of $2''$–$10''$. The sampling of this data set is too sparse to search for periodicities or determine the overall characteristics of the light curve, but a comparison with the VLA monitoring data indicates that the brightest flux densities at 1.3 mm occurred at times when the flux densities at centimeter wavelengths were also high (Zhao et al. 2003; see Fig. 2). In the future, more frequent SMA observations of Sgr A* at 1.3 and 0.87 mm will enable a comparison of the light curves at millimeter and centimeter wavelengths in more detail.

Finally, it has also been suggested that there may be a correlation between the radio flux density of Sgr A* and the closest approaches of orbiting stars. Loeb (2004) has predicted that the flux density of Sgr A* will vary on timescales greater than 1 month due to fluctuations in the mass accretion rate as stars approach and recede from Sgr A*. The predicted magnitude of an outburst, as well as the time delay between closest approach and the outburst are highly uncertain. Ghez et al. (2003a) have identified three periapse dates for massive stars in the Galactic center: SO-19 (1995.639), SO-16 (2000.243), and SO-2 (2002.335). Only the periapse for SO-2 occurred during our monitoring campaign (near day 685). We see no evidence in the light curves for an outburst occurring within

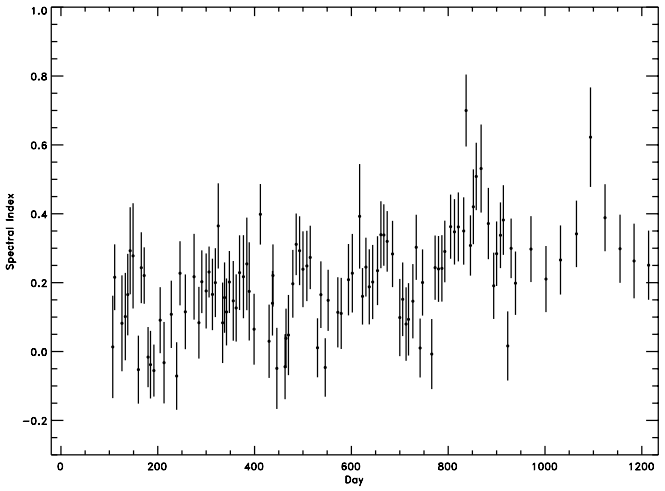

FIG. 7.—Spectral index α ($S_\nu \propto \nu^\alpha$) as a function of day for every epoch in which flux density measurements were obtained at all three wavelengths.

100 days of the SO-2 periapse. There is also no evidence for an increase in the mean flux density or a change in the spectral index on this timescale. Therefore, we conclude that the emission from Sgr A* at centimeter wavelengths is not significantly affected on timescales $\gtrsim$1 week by the close approach of massive stars.

4.1. *Spectral Index–Flux Density Correlation*

The spectral index α (defined as $S_\nu \propto \nu^\alpha$) can be calculated from the measured flux densities at 2.0, 1.3, and 0.7 cm. In Figure 7, we plot the calculated spectral index at every epoch in which the flux density was determined at all three wavelengths. The calculated values for α are also listed in Table 2. During the monitoring campaign, the spectral index was observed to vary between -0.07 ± 0.12 and 0.70 ± 0.10. The standard deviation of the calculated spectral indices is 0.14. In Figure 8, the spectral index is plotted as a function of the observed flux density at 0.7 cm ($S_{0.7}$). The spectral index depends linearly on $S_{0.7}$, with a best fit of $\alpha = -0.41(\pm 0.04) + 0.57(\pm 0.04)S_{0.7}$. The tendency toward steeper spectral index during outburst states is consistent with recent observations in the submillimeter (Zhao et al. 2003).

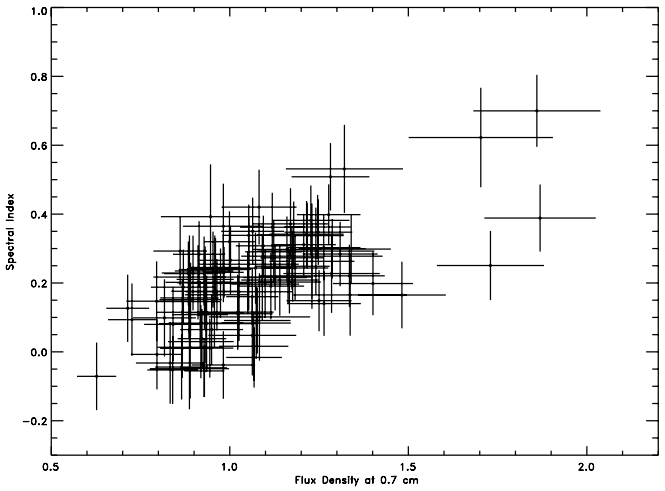

FIG. 8.—Spectral index α ($S_\nu \propto \nu^\alpha$) as a function of flux density at 0.7 cm. The spectral index becomes steeper during outbursts of Sgr A*.

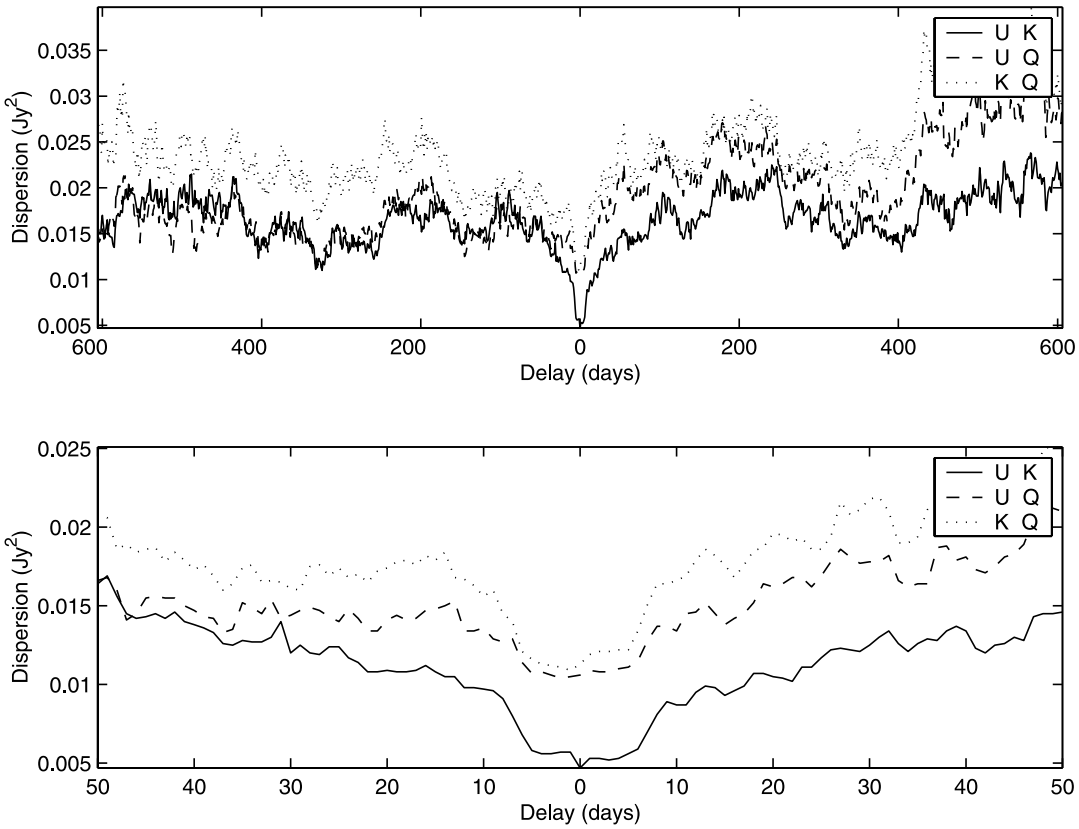

FIG. 9.—Dispersion as a function of time delay between pairs of light curves at the three different frequencies ($U = 2.0$ cm, $K = 1.3$ cm, and $Q = 0.7$ cm). There is a clear minimum in the dispersion at zero delay for each pair.

Increased fractional variability toward shorter centimeter wavelengths has been used to suggest that the observed variability of Sgr A* is intrinsic to the source (Zhao et al. 1992). The linear dependence of spectral index on 0.7 cm flux density strongly favors a model in which the observed variability is intrinsic to Sgr A* and not the result of interstellar scattering. If the flux density variability is caused by an outburst with a self-absorbed synchrotron spectrum (with $\alpha_{\rm sync} \approx 2$), then the flux density and the spectral index will rise together (e.g., Marscher & Gear 1985). For our data, the peak spectral index will occur when the self-absorption frequency is equal to 43 GHz (0.7 cm). At this point, the flux density at this frequency will also be at a maximum. As the self-absorption frequency moves to lower frequencies, both the spectral index and the 0.7 cm flux density will decrease, producing a correlation between spectral index and flux density. If the optically thin spectral index is $\ll 0$, then the spectral index will quickly become negative when the self-absorption frequency moves to lower frequencies. Because the measured spectral indices for Sgr A* are almost all greater than zero, the optically thin spectral index must be reasonably flat ($\alpha_{\rm thin} \gtrsim -0.5$).

Although we believe the above interpretation represents the most likely scenario, it is not unique. Due to the complexity and peculiarity of the Galactic center scattering screen, interstellar scattering cannot be ruled out as the source of the observed variability. However, a positive correlation between flux density and spectral index is not generally expected for interstellar scintillation. In simple models of interstellar scattering, the modulation index of the flux density decreases with frequency in the strong scattering regime (Rickett 1990). This would lead to an anticorrelation between spectral index and flux density. Furthermore, the timescale for diffractive scintillation for Sgr A* is less than 100 s while the timescale for refractive scintillation is 3×10^6 s, assuming relative velocities for the Earth and the scattering medium of $\sim$100 km s^{-1} (Rickett 1990). We detect strong variability on a timescale that falls well in between these characteristic times. Refractive scintillation appears to be only relevant for velocities greater than 1000 km s^{-1}, which would likely be associated with stellar winds in the central parsec or the accretion flow itself. To match the correlation (and the increased variability at millimeter and submillimeter wavelengths), the turbulence must increase substantially with decreasing scale size in the scattering medium.

The mean spectral index of Sgr A* can be calculated using the average flux densities at all three wavelengths (see Table 3). The best fit to the mean spectral index is $\alpha = 0.20 \pm 0.01$. There is strong evidence for a break in the spectrum of Sgr A* resulting in an excess in the flux density observed at 1 mm (Zylka, Mezger, & Lesch 1992; Serabyn et al. 1997; Falcke et al. 1998; Zhao et al. 2003). Falcke et al. (1998) calculate a spectral index of $\alpha = 0.17$ at wavelengths longer than 2 cm, but find a spectral index of $\alpha = 0.3$ at wavelengths of 2 cm and shorter. This measurement is based on a single epoch of data, and it is not unexpected given the observed standard deviation of the spectral index of 0.14 during our monitoring campaign. Large changes in the spectral index of Sgr A* can be seen in our data, and many epochs have spectral indices $\geq$0.3 (see Table 2). Our data, however, suggest that, on average, the break occurs at wavelengths shorter than 7 mm. Zhao et al. (2003) also find a spectral index of 0.1 ± 0.1 between 2.0 cm and 3 mm using one epoch of VLA data at 2.0,

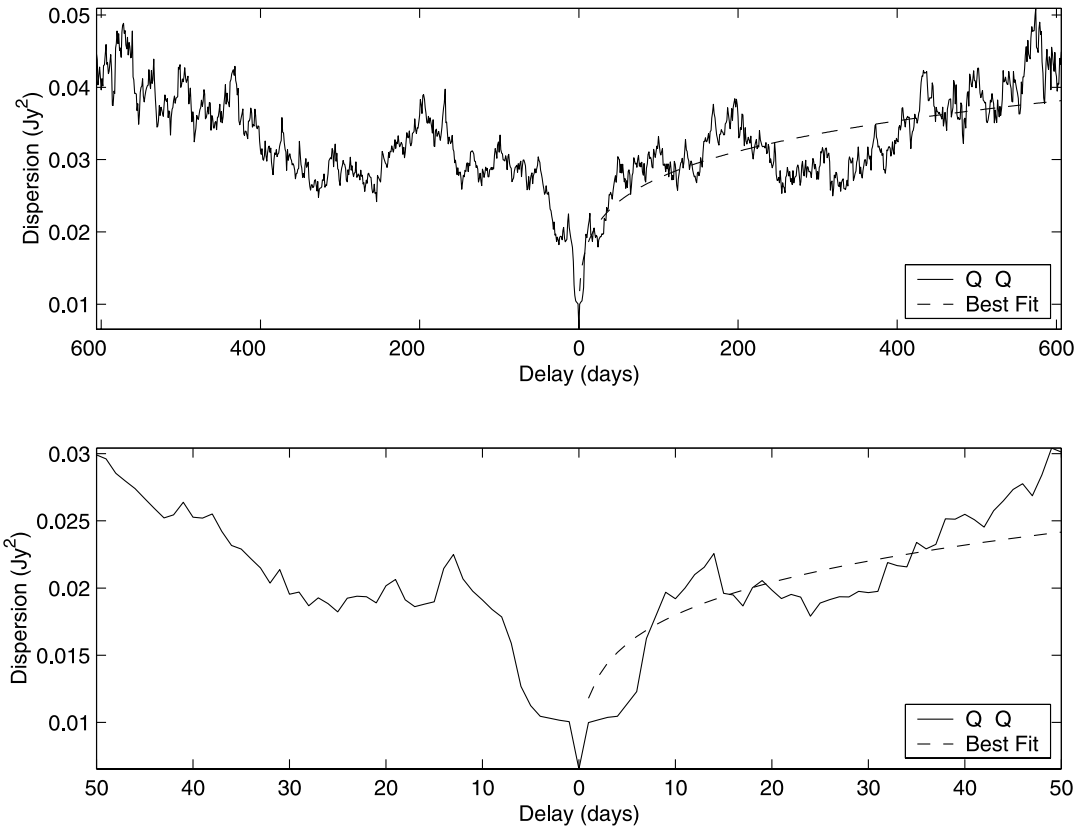

FIG. 10.—Autodispersion as a function of time delay for the 0.7 cm light curve. A power-law fit of $D^2 \propto t^{0.2}$ is also shown.

1.3, and 0.7 cm and a measurement of the flux density at 3 mm made by Tsutsumi et al. (2002). Between 3 and 0.87 mm, the spectral index rises to 0.25, indicating that the break in the spectrum occurs near 3 mm. It appears that, like the spectral index, the wavelength of the break in the spectrum is likely variable. Coordinated observations from centimeter to submillimeter wavelengths will be necessary to determine the precise characteristics of the break in the spectrum of Sgr A*.

A prolonged period of increased spectral index and 0.7 cm flux density appeared to begin around 2002 September 1 and has persisted throughout the remainder of the monitoring campaign. This period also corresponds to the time of an observed increase in variability of Sgr A* (see § 4). Before 2002 September 1 (day 805), the weighted mean spectral index was 0.16 ± 0.01 with a standard deviation of 0.11. The mean flux density at 0.7 cm was 0.94 ± 0.01 Jy. After September 1, the weighted mean of the spectral index and flux density at 0.7 cm increased to 0.33 ± 0.02 and 1.20 ± 0.02 Jy, respectively. The spectral index is also more variable during this time and has a standard deviation of 0.14.

4.2. *Time Delay*

The time sampling of our monitoring campaign makes our data sensitive to delays between wavelengths roughly greater than 1 week. The time delay between the flux density at the three different frequencies is estimated using the nonparametric method of Pelt et al. (1994). This method is used to calculate the dispersion between two irregularly sampled light curves by searching for a magnification and a shift in time of the two curves. The dispersion is essentially the mean square difference between the flux density at two frequencies on a given timescale. Figure 9 shows the dispersion between the light curves for each possible pair of wavelengths. The results strongly favor no delay between any pair of the three frequencies. A minimum is found in the dispersion for delays less than $\sim$5 days, which corresponds to the minimum sampling interval in our data. A monitoring campaign with sampling intervals on daily to hourly timescales will be necessary to determine time delays between wavelengths.

We also calculate the autodispersion of the data by comparing each light curve with itself. This calculation enables us to estimate the characteristic change in flux density with time. Results for all three wavelengths are similar, and the autodispersion for the 0.7 cm light curve is shown in Figure 10. The autodispersion grows slowly with time ($D^2 \propto t^{0.2}$). The weak dependence on time is consistent with the fairly static mean flux density that has been observed since the discovery of Sgr A* (e.g., ZBG01; Bower et al. 2002).

5. CONCLUSIONS

In this paper, we have presented results from a 3.3 yr campaign to monitor the flux density of Sgr A* at centimeter wavelengths using the VLA. The largest amplitude variations are observed at 0.7 cm, consistent with variability increasing toward shorter wavelengths (ZBG01). Overall, however, Sgr A* appears to be more quiescent than during previous monitoring campaigns. The spectral index of Sgr A* appears to be strongly correlated with the 0.7 cm flux density. This result strongly favors an emission mechanism in which outbursts are intrinsic to Sgr A* and are not the result of interstellar scintillation. Regular monitoring of Sgr A* at the VLA will continue through at least 2004 June with monthly observations at 2.0, 1.3, and 0.7 cm. These additional data will be useful in detecting periods longer than 100 days.

Much of the activity of Sgr A* appears to take place on timescales $\gtrsim$1 hr and less than the time resolution of our data (8 days). However, the monitoring campaigns in the radio and submillimeter have only minimally probed these timescales. To date, hourly timescales have only been systematically probed in X-rays and the infrared. In both cases, there is significant variability on timescales of hours. Monitoring of the centimeter flux density on these short timescales will be necessary to determine the duration and shape of outbursts, as well as detect any time lag between wavelengths. Additional coordinated multiwavelength campaigns specifically aimed at probing these timescales should also be implemented. Only with simultaneous coverage and fine sampling will we be able to ascertain the relationship between radio outbursts and X-ray flares and constrain the emission mechanism for Sgr A*.

The authors would like to thank C. Fassnacht for help with the initial data calibration and sharing his code to calculate the dispersion between light curves. We also thank C. Chandler for the model image of 3C 286 used in the data calibration and J. Herrnstein for useful discussions.

REFERENCES

Baganoff, F. K. 2003, BAAS, 35, 03.02
Baganoff, F. K., et al. 2001, Nature, 413, 45
Bower, G. C., Falcke, H., Herrnstein, R. M., Zhao, J.-H., Goss, W. M., & Backer, D. C. 2004, Science, in press
Bower, G. C., Falcke, H., Sault, R. J., & Backer, D. C. 2002, ApJ, 571, 843
Brown, R. L., & Lo, K. Y. 1982, ApJ, 253, 108
Falcke, H. 1999, in ASP Conf. Ser. 186, The Central Parsecs of the Galaxy, ed. H. Falcke, A. Cotera, W. J. Duschl, F. Melia, & M. J. Rieke (San Francisco: ASP), 113
Falcke, H., Goss, W. M., Matsuo, H., Teuben, P., Zhao, J., & Zylka, R. 1998, ApJ, 499, 731
Genzel, R., Schödel, R., Ott, T., Eckart, A., Alexander, T., Lacombe, F. D. R., Rouan, D., & Aschenbach, B. 2003, Nature, 425, 934
Ghez, A. M., Becklin, E., Duchêne, G., Hornstein, S., Morris, M., Salim, S., & Tanner, A. 2003a, in Proc. Galactic Center Workshop 2002, ed. A. Cotera, H. Falcke, T. R. Geballe, & S. Markoff (Astron. Nachr. Suppl. S1) (New York: Wiley), 527
Ghez, A. M., et al. 2003b, ApJ, 586, L127
Goldwurm, A., Brion, E., Goldoni, P., Ferrando, P., Daigne, F., Decourchelle, A., Warwick, R. S., & Predehl, P. 2003, ApJ, 584, 751
Loeb, A. 2004, MNRAS, in press
Marscher, A. P., & Gear, W. K. 1985, ApJ, 298, 114
Menten, K. M., Reid, M. J., Eckart, A., & Genzel, R. 1997, ApJ, 475, L111
Pelt, J., Hoff, W., Kayser, R., Refsdal, S., & Schramm, T. 1994, A&A, 286, 775
Porquet, D., Predehl, P., Aschenbach, B., Grosso, N., Goldwurm, A., Goldoni, P., Warwick, R. S., & Decourchelle, A. 2003, A&A, 407, L17
Press, W. H., Flannery, B. P., Teukolsky, S. A., & Vetterling, W. T. 1989, Numerical Recipes in C: The Art of Scientific Computing (Cambridge: Cambridge Univ. Press)
Rickett, B. J. 1990, ARA&A, 28, 561
Schödel, R., et al. 2002, Nature, 419, 694
Serabyn, E., Carlstrom, J., Lay, O., Lis, D. C., Hunter, T. R., & Lacy, J. H. 1997, ApJ, 490, L77
Tsuboi, M., Miyazaki, A., & Tsutsumi, T. 1999, in ASP Conf. Ser. 186, The Central Parsecs of the Galaxy, ed. H. Falcke, A. Cotera, W. J. Duschl, F. Melia, & M. J. Rieke (San Francisco: ASP), 105
Tsutsumi, T., Miyazaki, A., & Tsuboi, M. 2002, BAAS, 34, 950
Wright, M. C. H., & Backer, D. C. 1993, ApJ, 417, 560
Zhao, J.-H., Bower, G. C., & Goss, W. M. 2001, ApJ, 547, L29 (KBG01)
Zhao, J.-H., Goss, W. M., Lo, K.-Y., & Ekers, R. D. 1992, in ASP Conf. Ser. 31, Relationships Between Active Galactic Nuclei and Starburst Galaxies, ed. A. V. Filippenko (San Francisco: ASP), 295
Zhao, J.-H., Herrnstein, R. M., Bower, G. C., Goss, W. M., & Liu, S. M. 2004, ApJ, 603, L85
Zhao, J.-H., Young, K. H., Herrnstein, R. M., Ho, P. T. P., Tsutsumi, T., Lo, K. Y., Goss, W. M., & Bower, G. C. 2003, ApJ, 586, L29
Zylka, R., Mezger, P. G., & Lesch, H. 1992, A&A, 261, 119